

# Observation of diffractive orbits in the spectrum of excited NO in a magnetic field

A. Matzkin

Laboratoire de Spectrométrie physique (CNRS Unité 5588),  
Université Joseph-Fourier Grenoble-I, BP 87, 38402 Saint-Martin, France

M. Raoult

Laboratoire Aimé Cotton (CNRS Unité 3321), Université de Paris-Sud, 91405 Orsay, France

D. Gauyacq

Laboratoire de Photophysique moléculaire (CNRS Unité 3361), Université de Paris-Sud, 91405 Orsay, France

We investigate the experimental spectrum of excited NO molecules in the diamagnetic regime and develop a quantitative semiclassical framework to account for the results. We show the dynamics can be interpreted in terms of classical orbits provided that in addition to the geometric orbits, diffractive effects are appropriately taken into account. We also show how individual orbits can be extracted from the experimental signal and use this procedure to reveal the first experimental manifestation of inelastic diffractive orbits.

PACS numbers: 32.60.+i 03.65.Sq 32.55.Be 05.45.Mt

Periodic orbit (PO) theory [1] has been a very successful quantitative and qualitative tool in the analysis of systems displaying strong quantum fluctuations. In particular, the complex photoabsorption spectrum of excited hydrogen atoms in a static magnetic field was interpreted within closed orbit theory (COT) in terms of periodic orbits *closed* at the nucleus [2]. However standard PO theory was shown to be insufficient for systems containing a scatterer smaller or comparable to one de Broglie wavelength, because the PO's may hit the scatterer, thereby producing *diffractive* orbits [3]. In certain mesoscopic devices diffractive orbits crucially influence the spectrum [4], whereas in non-hydrogenic Rydberg atoms in static fields the atomic core acts as a scatterer producing combination orbits [5]. This was experimentally observed in the photoabsorption spectrum of helium, which departs slightly from the hydrogenic case [6]. In the case of Rydberg molecules, core effects are expected to be more important: the reason is that the diffractive scatterer has an internal structure (the quantum states of the molecular core). Indeed, model calculations recently predicted that Rydberg molecules in external fields would display a novel type of diffractive orbit produced by inelastic scattering of the PO's on the core [7].

In this work, we address this problem by investigating the experimental spectrum of excited NO molecules in a magnetic field. We show the apparently complex spectrum can be well understood in terms of closed orbits provided molecular core effects are appropriately taken into account; in particular, we shall see COT calculations correctly reproduce the Fourier transform of the experimental spectrum, in a regime in which quantum calculations have yet to be undertaken. We will also demonstrate how individual orbits may be extracted from the experimental results by using a modified Fourier transform, and use this technique to show the first experimental manifestation of

an *inelastic diffractive* orbit in a physical system.

Most previous studies of atoms in a magnetic field have relied on scaled-energy spectroscopy, in which the field  $B$  is varied with the Rydberg electron energy  $E$  so as to keep the scaled energy  $\epsilon = E(B/B_0)^{-2/3}$  constant, with  $B_0 = 2.35 \times 10^5$  T. Then the classical motion is unchanged at each point of the spectrum and each orbit contributes as a peak in the Fourier transformed (FT) spectrum. However, such a scaling law does not hold, albeit approximately, for molecules. We have therefore observed the Rydberg states of NO at a constant magnetic field of 0.93 T, varying the excitation energy of the probe laser. The experiment, carried out in a "magnetic bottle" time of flight spectrometer, was described elsewhere [8], but in short: a 2-photon highly selective transition with a pump laser brings the molecule from the ground state  $X^2\Pi_{3/2}$  (in the vibrational level  $v'' = 0$ ) into the single

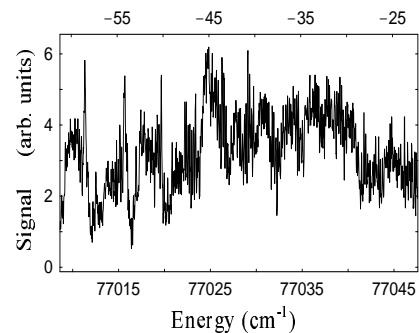


FIG. 1: Experimental spectrum for the transition from the  $A^2\Sigma^+$ ,  $N = 3$ ,  $M_N = -3, \dots, 3$  states of NO in a static magnetic field of strength  $B = 0.93$  T. The lower scale gives the energy relative to the ground state of NO. The origin of the upper scale corresponds to the field-free ionization threshold for levels converging to the  $N^+ = 1$  rotational state of  $\text{NO}^+$ .

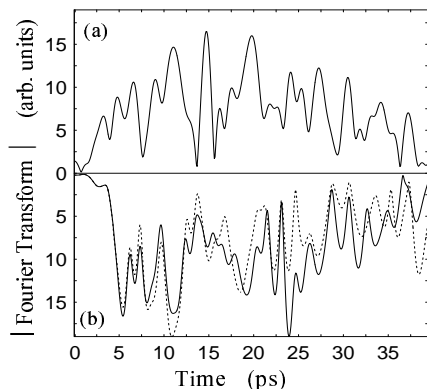


FIG. 2: (a) Fourier-transform of the experimental spectrum. The first peak (marked with a star) is a residual oscillation from the background due to the redistribution of the oscillator strength into molecular Zeeman structures at low energies [9]. (b) Closed-orbit semiclassical calculations with (solid line) and without (dotted line) the diffractive contributions. An independent calculation was performed for each value of  $M_N$ ; each result was then multiplied by the relative weight of the  $M_N$  component before taking the Fourier transform. Note that the wide peaks are not correlated with single closed orbits but arise from a coherent superposition of orbits at different energies. The shortest contributing orbit is an orbit perpendicular to the field with a period of 4.22 ps.

rotational Zeeman sublevel  $N = 3$   $M_S = 1/2$  of the first electronic excited state  $A^2\Sigma^+$ ,  $v' = 1$ ;  $N$  is the total angular momentum exclusive of spin and the constant spin number  $M_S$  will henceforth be disregarded. The sublevels  $M_N = -3$  to  $3$  (where  $M_N$  is the projection of  $N$  on the field axis) were not resolved but their relative population is known. In a second step, the probe laser, linearly polarized parallel to the field axis, excites the molecules to high-lying Rydberg states having also  $v = 1$  (so we can neglect vibrational couplings).

These excited states are further ionized via vibrational autoionization into the ground state of the  $\text{NO}^+$  core. The resulting spectrum, which lies higher in energy than those previously published in [8] (in which nonperturbative diamagnetic effects could be neglected), is shown in Fig. 1. The FT of the experimental spectrum is shown in Fig 2(a), whereas Fig. 2(b) displays the semiclassical calculations which will be detailed below. Unlike a spectrum taken at constant  $\epsilon$ , we do not expect in the present case to correlate each peak with a single orbit, because the period of an orbit changes with the energy. Before turning to the extraction of individual orbits, we detail the mechanism giving rise to the peaks in the FT spectrum.

Since in the  $A^2\Sigma^+$  state the orbital momentum of the Rydberg electron is a mixture of both  $l = 0$  and  $l = 2$ , the probe laser excites to final states having  $l = 1, 3$  and  $N = 2, 3, 4$ . Photo-excitation takes place in the molecular frame (in which the Rydberg electron is coupled to

the molecular core), but following excitation the electron uncouples from the core and  $N$  is no longer conserved, although its projection  $M_N$  is [10]. The molecule is then described as an electron orbiting around the molecular core  $\text{NO}^+$  in well-defined rotational states  $N^+ = 1, 3$  or  $5$ . For each core configuration, the electron's wavefunction is propagated semiclassically along classical trajectories (see Fig. 3). The energy of the Rydberg electron

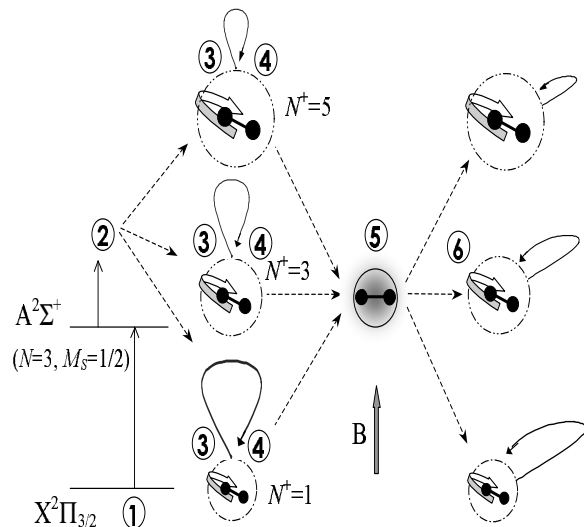


FIG. 3: Schematic diagram of the excitation dynamics of the Rydberg states of  $\text{NO}$  in a magnetic field. (1) A pump laser excites the molecules from the ground state  $X^2\Pi_{3/2}$  to the intermediate state  $A^2\Sigma^+$ ,  $N = 3$ , via a 2-photon transition. A high-resolution probe laser then excites the molecules from the intermediate state to Rydberg levels with orbital momentum  $l = 1$  and  $l = 3$ . (2) Following this excitation the Rydberg electron uncouples from the molecular core which is left freely rotating with rotation quantum numbers  $N^+ = 1, 3$  or  $5$ . (3) As the Rydberg electron leaves the core region its dynamics is described using classical trajectories; the molecular energy is partitioned between the Rydberg electron and the core: as the core rotation increases (pictured by a larger core), the energy of the Rydberg electron decreases (symbolized by smaller orbits). The core region is less than 5 a.u. large, whereas even the shortest orbit associated with a highly rotating core in state  $N^+ = 5$  extends beyond 1500 a.u. (4) Some trajectories return to the core, which following the terminology of diffractive PO theory we call the *geometric closed orbits*; they are the same orbits that exist in the diamagnetic hydrogen atom (i.e. in the absence of the core). (5) As the Rydberg electron enters the core region, its dynamics recouples with the core. The waves carried by the geometric CO's overlap with the initially-dipole excited waves, producing fluctuations in the oscillator strength. (6) The electron scatters off the core, uncouples, and follows again classical trajectories; during the scattering process, the electron may have exchanged energy with the core. Eventually, some trajectories return once more to the core; these *diffractive orbits*, composed of 2 geometric CO's connected by elastic or inelastic core-scattering, produce further fluctuations in the oscillator strength.

$N^+$	1	3	5
$\epsilon$	-1.1 $\rightarrow$ -0.4	-1.5 $\rightarrow$ -0.7	-2.1 $\rightarrow$ -1.4
$ \mathcal{Q}_{N^+}^G $	0.133	0.304	0.225
$ \mathcal{Q}_{N^+,3}^D $	0.004	0.264	0.003

TABLE I: For each state of the core, we give the range of the scaled energy  $\epsilon$  of the Rydberg electron as the probe laser is scanned. When  $N^+ = 5$ , the very low values of  $\epsilon$  correspond to the near integrable regime. For  $N^+ = 3$ , the dynamics of the Rydberg electron is mostly regular. For  $N^+ = 1$ , the electron enters the chaotic regime: at  $\epsilon = -0.4$ , about 50 % of the classical phase space is chaotic [12]. We also give the modulus of  $\mathcal{Q}^G$  and  $\mathcal{Q}^D$  for  $N^+ = 3$  and for  $M_N = -1$ ; these values give a rough idea of the PO-independent part of the fluctuations strength associated with the different geometric and diffractive contributions.

is obtained from the energy partition

$$E_{N^+} = E_{N^+=1} + B_r [N^+(N^+ + 1) - 2] + \frac{m_l}{2} B/B_0, \quad (1)$$

where  $B_r$  is the rotational constant of  $\text{NO}^+$ . Disregarding the linear Zeeman shift, we have three main dynamical regimes for the Rydberg electron, each associated with a different rotational core state. Table I gives, for each value of  $N^+$  the scaled energy ranges corresponding to the experimental spectrum.

At each energy  $E_{N^+}$ , some of the trajectories are turned back by the field and return to the core; those trajectories are the *geometric closed orbits*. Their contribution to the oscillator strength  $f(E)$  is given by [9]

$$\sum_{N^+} \mathcal{Q}_{N^+}^G \sum_k \mathcal{A}_k(E_{N^+}) \exp[i\mathcal{S}_k(E_{N^+})]. \quad (2)$$

$\mathcal{A}_k$  and  $\mathcal{S}_k$  are 3-dimensional quantities respectively linked to the 2-dimensional classical amplitude  $A_k$  and action  $S_k$  of the  $k$ th closed orbit [11] ( $\mathcal{S}_k$  includes the Maslov index  $\mu_k(E_{N^+})$ ); those quantities depend on the energy of the Rydberg electron, i.e. on the core state and on the excitation energy.  $\mathcal{Q}_{N^+}^G$  is a quantity depending on the dipole transition factor from the  $A^2\Sigma^+$  to the excited states, and on the transformation elements from the coupled to the uncoupled frame; some values are given in Table I.

When the semiclassical wavefunction carried by the geometric closed orbits returns to the core, it diffracts on the scatterer (Fig. 3). This diffraction process, produces newly outgoing trajectories  $q$ , which eventually return to the core; the resulting diffractive contribution to  $f(E)$  is given by

$$\sum_{N^+, N^+'} \mathcal{Q}_{N^+, N^+}^D \sum_{k, q} \mathcal{A}_k(E_{N^+}) \mathcal{A}_q(E_{N^+}') \times \exp i[\mathcal{S}_k(E_{N^+}) + \mathcal{S}_q(E_{N^+}')]. \quad (3)$$

$\mathcal{Q}_{N^+, N^+}^D$  acts as a global diffraction coefficient; unlike diffraction in quantum billiards [3, 4],  $\mathcal{Q}_{N^+, N^+}^D$  does not depend here on the local geometry of the scatterer but solely on the quantum properties of the core (i.e. on the core-induced phase-shifts, known as molecular quan-

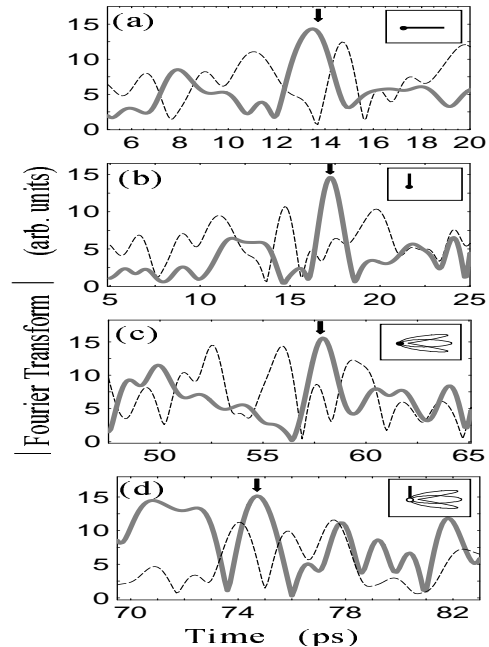


FIG. 4: Extraction of individual orbits from the experimental spectrum using the chirped FT procedure. In the present illustration, we show the results for 4 orbits which exist at an excitation energy  $E_0 = -26.91 \text{ cm}^{-1}$  below the field free  $N^+ = 1$  ionization threshold. (a) Extraction of the second return of the perpendicular orbit ( $R_2$  in the nomenclature given e.g. in [14]), associated with the core in state  $N^+ = 5$ ; the corresponding scaled energy of this orbit is  $\epsilon = -1.49$ . *Broken curve*: standard FT of the experimental spectrum, shown in Fig. 1. *Thick curve*: chirped FT of the experimental spectrum obtained by calculating the function  $\xi(t; E)$  appearing in Eq. (4) for this orbit. The arrow indicates the calculated classical period of  $R_2$ , which agrees very well with the position of the peak appearing in the CFT. (b) CFT extraction of the orbit  $V_1$ , parallel to the field axis, associated with the core in state  $N^+ = 3$ , at  $\epsilon = -0.85$ . (c) Extraction of the  $R_3^1$  orbit associated with the core in state  $N^+ = 1$ ; orbits associated with  $N^+ = 1$  are generically more difficult to extract from the experimental signal because the oscillator strength tends to be dominated by orbits associated with  $N^+ = 5$  and 3 (see Table I). However, at this energy, corresponding to  $\epsilon = -0.48$ , the classical amplitude  $A_{R_3^1}$  is very strong (because  $\epsilon$  is close to the bifurcation energy at which this orbit is created [15]), thereby allowing the signal to pick up its contribution. (d) By applying the CFT procedure to the action expansion  $S_{V_1}(E_{N^+=3}) + S_{R_3^1}(E_{N^+=1})$ , we can also extract the *diffractive orbit* formed by the combination of the orbits extracted in (b) and (c); the period of the diffractive orbit is given by summing the periods of the two geometric CO's. The shape of the orbits is given in the upper right-hand side of each plot ( $B$  is in the vertical direction).

tum defects; the value of the 6 independent quantum defects for NO is given in [8]). The matching between the semiclassical waves and the core wavefunction takes place in the stationary phase approximation. The oscillator strength contains both elastic ( $N^+ = N^{+'}$ ) and inelastic ( $N^+ \neq N^{+'}$ ) diffractive terms. In the one core-scatter approximation, the total contribution to the fluctuations in the oscillator strength is obtained by summing the imaginary parts of Eqs. (2) and (3).

The experimental or semiclassically calculated FT spectra  $|\mathcal{F}(t; \xi)|$  are respectively obtained by Fourier transforming the photoelectron signal or the oscillator strength for which we shall use the same notation  $f(E)$ , hence

$$\mathcal{F}(t; \xi) = \int_{E_{\min}}^{E_{\max}} f(E) \exp(-i\xi(t, E)) dE \quad (4)$$

where  $\xi(t, E) = Et$ , and we set the energy variable relative to the  $N^+ = 1$  ionization threshold as  $E = E_{N^+=1}$ . The semiclassical calculations were undertaken by applying Eqs. (2) and (3). Since at each point  $E_0$  of the spectrum the orbits and therefore their amplitude and action change, we have determined the classical quantities  $A_k$ ,  $S_k$ ,  $\mu_k$  on an energy grid for the primitive closed orbits and their repetitions, keeping track of bifurcations as the energy increases. We then interpolated those functions so as to obtain classical quantities varying with the energy. This procedure, which is tractable for short orbits provided the scaled energy is not too high, yields a good agreement with the experimental FT spectrum, as seen on Fig. 2(b). The semiclassical calculations allow to single out contributions from the ensemble of geometric or diffractive orbits associated with given core states. Full details will be given elsewhere [9].

Eq. (4) is also at the basis of the extraction of *individual orbits* from the experimental spectrum provided  $\xi(t, E)$  is appropriately modified so as to counterbalance the varying values of the classical quantities. Indeed in the neighborhood of some energy  $E_0$  a classical orbit  $k$  contributes locally as a sinusoidal oscillation of period  $T_k(E_0)$ . But as the energy is varied, the classical motion changes, turning the sinusoidal oscillation into a chirped modulation. It has been shown very recently [13] that a chirped Fourier Transform (CFT) converts a chirp modulation into a sine oscillation, thus giving a sharp peak in the FT spectrum. A CFT is defined by setting  $\xi(t, E) = t(E - E_0) + b(E - E_0)^2 + c(E - E_0)^3 + i \ln \alpha(E - E_0)$  in Eq. (4).  $b$  and  $c$  are numerical coefficients and  $\alpha$  is a function, which depend on the orbit to be extracted: to extract an orbit  $k$  at some energy  $E_0$ , we Taylor expand the action  $S_k(E)$ . To first order, we have  $\partial_E S(E_0) = T_k(E_0)$ , i.e. the period of the orbit. Therefore by setting  $b = -\partial_E^2 S_k(E_0)/2$  and  $c = -\partial_E^3 S_k(E_0)/6$

in the CFT exponent  $\xi$ , we can expect to effectively linearize the signal around  $E_0$  so that the CFT yields a peak at  $t = T_k(E_0)$ . The peak can be enhanced by using a function  $\alpha$  to compensate for the signal amplitude variation; we have used the inverse of our interpolated functions  $A_k(E)$ . As discussed in great details in [13], spurious peaks inevitably appear in the CFT spectrum. We proceed in the following manner: using purely classical calculations, we compute on the one hand the CFT of the experimental signal with the relevant parameters  $a, b$ , and  $\alpha$ , and on the other hand we determine the period  $T_k(E_0)$ ; the consistency of the procedure is ensured by the appearance of a peak at the computed value  $t = T_k(E_0)$  when the orbit is successfully extracted from the signal. An illustration of the extraction procedure is given in Fig. 4. For a fixed energy  $E_0$  we extract one CO associated with each core state (panels (a)-(c)). Panel (d) shows the extraction of the diffractive CO formed by the combination of the orbits extracted in (b) and (c).

In summary, we have investigated the experimental spectrum of NO in the diamagnetic regime and interpreted the results in terms of geometric and diffractive classical orbits, and we have shown how individual orbits can be extracted from the experimental signal.

- 
- [1] M. C. Gutzwiller, *Chaos in classical and quantum mechanics* (Springer, New-York, 1990).
  - [2] M. L. Du and J. B. Delos, Phys. Rev. A **38**, 1913 (1988).
  - [3] G. Vattay, A. Wirzba and P.E Rosenqvist, Phys. Rev. Lett. **73**, 2304 (1994).
  - [4] J. S. Hersch, M. R. Haggerty, and E. J. Heller, Phys. Rev. Lett. **83**, 5342 (1999).
  - [5] P. A. Dando, T. S. Monteiro, D. Delande and K. T. Taylor, Phys. Rev. Lett. **74**, 1099 (1995).
  - [6] K. Karremans, W. Vassen, and W. Hogervorst, Phys. Rev. Lett. **81**, 4843 (1998).
  - [7] A. Matzkin, P. A. Dando, and T. S. Monteiro, Phys. Rev. A **66**, 013410 (2002).
  - [8] D. Gauyacq, M. Raoult and N. Shafizadeh, in C. Sandorfy (Ed.), *The Role of Rydberg States in Spectroscopy and Photochemistry* (Kluwer, Dordrecht, 2002); M. Raoult, S. Guizard and D. Gauyacq, J. Chem. Phys. **94**, 7046 (1991).
  - [9] M. Raoult, D. Gauyacq, S. Guizard and A. Matzkin, in preparation.
  - [10] T. S. Monteiro and K. T. Taylor, J. Phys. B **23**, 427 (1990).
  - [11] J. Gao, J.B. Delos, and M. Baruch, Phys. Rev. A **46**, 1449 (1992).
  - [12] H. Friedrich and D. Wintgen, Phys. Rep. **183**, 37 (1989).
  - [13] S. Freund, R. Ubert, E. Flöthmann, K. Welge, D. M. Wang and J. B. Delos Phys. Rev. A **65**, 053408 (2002).
  - [14] J. Main, Phys. Rep. **316**, 233 (1999).
  - [15] J.M. Mao and J. B. Delos Phys. Rev. A **45**, 1746 (1992).